Available online at www.sciencedirect.com
ScienceDirect
Catalysis Today 126 (2007) 412–419
CATALYSIS TODAY
www.elsevier.com/locate/cattod

Structure, thermal-stability and reducibility of Si-doped Ce–Zr–O solid solution

Xiaohong Wang, Guanzhong Lu *, Yun Guo, Yuye Xue, Liangzhu Jiang, Yanglong Guo, Zhigang Zhang

Lab for Advanced Materials, Research Institute of Industrial Catalysis, East China University of Science and Technology, Shanghai 200237, PR China

Available online 13 July 2007

Abstract

The Si-doped Ce–Zr–O solid solutions have been prepared by the reverse microemulsion method. The effects of Si and its content on the structure characters, thermal-stability and reducibility of the Ce–Zr–O solid solution have been studied by N_2 adsorption, XRD, laser Raman (LR), TPR, FT-IR, NMR and XPS methods. The results indicate that, there are the bonds of Si–O–M (Ce or Zr) in the Ce–Zr–Si–O solid solutions, and the presence of Si can increase obviously the surface area, thermal-stability, crystal lattice distortion rate, and reducibility of the solid solution. The surface area of the sample with 20 wt.% Si reaches 153 $m^2\ g^{-1}$ after being calcined at 900 °C for 6 h. The Ce–Zr–O solid solution with 5.2–10 wt.% Si shows excellent thermal-stability and reducibility.

Keywords: Ce–Zr–O solid solution; Thermal-stability; Reducibility; Silicon doping; Oxygen activity

1. Introduction

The Ce–Zr–O solid solution or other ceria-based oxides is one of the key components in three-way catalysts (TWCs), and plays the important roles of the oxygen storage and textural promoters [1–3]. Under alternating lean and rich fuel conditions, these oxides can store and release oxygen thereby enabling TWCs to catalyze efficiently the oxidation of CO and volatile organic compounds and the reduction of NO_x. High catalytic performance of TWCs is associated with the high specific surface area, high thermal-stability and excellent oxygen exchange capacity for a release and uptake of oxygen. Therefore, the Ce–Zr–O solid solution must possess the high thermal-stability of textural structures, a single phase state at higher temperature and good removability of oxygen.

Generally speaking, the thermal-stability of textural structures and the oxygen activity of Ce–Zr–O solid solution can be promoted by adopting a suitable synthesis method, changing the atomic ratio of Ce/Zr and doping it with foreign elements.

Up to now, a great variety of methods have been investigated to improve the physicochemical properties of Ce–Zr–O solid solution, for which Kašpar et al. have reported a review article [4] and commented on the advantages and disadvantages of various preparation methods. The nanostructure materials of Ce–Zr–O with high properties can be prepared by adopting appropriate designs and synthesis, and will be used necessarily in the next generation of TWCs.

The effect of the atomic ratio of Ce/Zr on the properties of Ce–Zr–O solid solution has also been studied by many researchers. It has been proved that, when the atomic ratio of Zr/Ce closes to 1, the Ce–Zr–O solid solution with a tetragonal symmetry behaves a high oxygen storage capacity (OSC) and high resistance to thermal sintering [5–9]. On the other hand, the properties of some mixed oxide ceramics and their solid solutions depend often on many factors, among which the chemical nonstoichiometry is of capital importance [10]. The studies show that doping Ce–Zr–O solid solution with other elements can affect significantly its structure characteristics and improve its oxygen storage capacity and catalytic activity. The presence of cations with smaller ionic radius near the Ce^{4+} ions in the solid solution makes an expansion of the lattices easier, and promotes the valence change between Ce^{4+} (0.097 nm) and Ce^{3+} (0.114 nm). Incorporating the cationic

* Corresponding author. Tel.: +86 21 64253703; fax: +86 21 64253703.
E-mail address: gzhlu@ecust.edu.cn (G.Z. Lu).

0920-5861/$ – see front matter
doi:10.1016/j.cattod.2007.06.009

dopants with an oxidation state of <+4 into the ceria lattices can lead to a formation of intrinsic oxygen vacancies to release the stress caused by the cation size mismatch. Schulz et al. [11] have synthesized Si- and Al-doped nanocrystalline Ce–Zr–O solid solution ($Ce_{0.5}Zr_{0.5}O_2$) by the flame–spray pyrolysis method, and proved that adding silica (up to 20 wt.%) or alumina (up to 16 wt.%) alters the particles morphology from polyhedral to spherical particles, but the roles of Si and Al in Ce–Zr–O solid solution is not clear. In doped Ce–Zr–O solid solution, the oxygen storage capacity (OSC) is affected much by the silica content but very little by the alumina content. Fernández-García et al. [12] have prepared Ce–Zr–Ca–O ternary mixed oxide by a microemulsion method, and found that an introduction of CaO into ceria–zirconia structure modifies strongly the surface and bulk oxygen storage capacity. Bulk oxygen diffusion is a function of the Ca content and slightly decays at low Ca content. Chen et al. [13] have prepared nano-sized Ce–Zr–Ba mixed oxide. As the promoter of TWCs, Ce–Zr–Ba mixed oxide offers better properties than that of Ce–Zr–O binary mixed oxide. Ikryannikova et al. [14] have studied the electron-accepting properties of Ce–(Pr)–Zr–O solid solution modified by Y^{3+} or La^{3+} and proved that an introduction of trivalent cation (Y^{3+} or La^{3+}) decreases the electron-accepting properties of Ce^{3+} ions on the surface.

As the ionic radius of Si^{4+} is only 0.026 nm that is much smaller than that of Ce^{4+}(0.097 nm), Ce^{3+}(0.114 nm) and Zr^{4+}(0.084 nm), its addition in Ce–Zr–O solid solution will make easily an expansion of the lattices and the valence change between Ce^{4+} and Ce^{3+}. This means that OSC of Ce–Zr–O solid solution can be promoted by silicon. Besides, silicon is very effective element for improving the thermal-stability of many composite oxides, such as alumina–substrate composite oxides [16]. Based on the reasons above, silica was chosen as an additive of Ce–Zr–O solid solution to improve its reducibility and thermal-stability. In this paper, a series of Si-doped Ce–Zr–O solid solutions were prepared by a reverse microemulsion method and the effect of Si on the structure characters, thermal-stability and reducibility of the Ce–Zr–O samples were investigated by N_2 adsorption, XRD, LR, TPR, NMR, FT-IR and XPS methods.

2. Experiments

Si-doped Ce–Zr–O solid solution (Ce/Zr = 1, atom) was prepared by the reverse microemulsion method described in detail in Refs. [15,16]. The reverse microemulsion (I) of cerium and zirconium nitrate, polyethylene glycol octylphenyl ether (as surfactant), cyclohexane (as oil phase), 1-hexanol (as co-surfactant) and ethyl silicate (as additive) was prepared; the reverse microemulsion (II) of ammonia, polyethylene glycol octylphenyl ether, cyclohexane, 1-hexanol and hydrogen peroxide (as oxidant) was prepared; the reverse microemulsion (I) was mixed with (II) to react; the precipitates was filtered from the matrix solution. And then the solid samples were dried and calcined in air at 550 °C for 5 h or 900 °C for 6 h. Pure Ce–Zr–O solid solution has also been prepared as a reference. The samples are signed as Ce–Zr–Si(X)–O, in which X represents the content of Si (wt.%).

The BET surface area and pore diameter distribution of the samples were measured at −196 °C with nitrogen as an adsorbent by the ST-03 type instrument of surface area and pore diameter distribution (Beijing).

The X-ray diffraction (XRD) patterns were measured on the Rigaku D/max-2550/PC diffractometer operated at 50 kV and 180 mA, with Cu Kα radiation (λ = 1.54056 Å) and a diffracted beam monochromator. The distortion rate of crystal lattice (e) was estimated by the equation of $e = 1/4\beta \operatorname{ctg} \theta$, where β is the corrected peak width.

Raman spectra were collected by a LabRam-1B spectrometer of Dilor Company, and 632.8 nm line of He–Ne was used.

Temperature-programmed reduction (TPR) of the samples was carried out in a conventional flow system equipped with a thermal conductivity detector (TCD). The sample was pretreated in N_2 at 500 °C for 1 h before TPR run. The composition of mixture gas was 8% H_2/N_2 (25 ml/min) and the heating rate is 600 °C/h. TT was defined as the temperature at peak top; HC, the amount of hydrogen consumption per cerium atom; OR, the amount of oxygen release per cerium atom; RD, the reduction degree (the ratio of $Ce^{3+}/(Ce^{4+} + Ce^{3+})$).

HC was estimated according to the area sum of all the reduction peaks, in which the area integrated was translated to the amount of hydrogen consumption by the criteria curves of hydrogen amount to the peak area. OR and RD were derived from HC according to the following reaction equation: $CeO_2 + H_2 = 1/2Ce_2O_3 + H_2O$. Here, 1 mol hydrogen is corresponded to 0.5 mol oxygen and 0.5 mol Ce^{3+}, and the amount of $Ce^{4+} + Ce^{3+}$ in the RD calculation is the total amount of cerium in the samples.

The solid-state ^{29}Si MAS NMR spectra were recorded on a Bruker AVANCE-500 spectrometer at 99.4 MHz, using 4 mm zirconium oxide rotor, a rotation frequency of 4000 Hz, and tetramethyl silane as an external standard.

The FT-IR spectra of samples were recorded on a Nicolet Nexus 670 FT-IR spectrometer, and the sample to be measured was ground with KBr and pressed into a thin wafer.

The X-ray photoelectron spectroscopy (XPS) spectra of sample was performed on a VC Escalab II spectrometer using monochromatic Mg Kα radiation ($h\nu$ = 1253.6 eV) at 1×10^{-10} Torr. Electrostatic surface charging was observed in all investigated samples owing to their poor electric conductivity. The binding energy (BE) of adventitious C_{1S} (284.8 eV) was used as a reference. The binding energy measured is accurate to ±0.2 eV. The surface composition of sample was calculated by the photoelectron peak area of each element in the XPS spectrum.

3. Results and discussion

3.1. BET surface area

The BET surface areas of Ce–Zr–O solid solutions and its loss after calcination at high temperature are listed in Table 1. In order to investigate the sintering of the samples at

Table 1
BET surface area of Ce–Zr–Si–O solid solution and its sintering degree after calcination at 900 °C for 6 h

Sample	Si content (wt.%)	Ce:Zr:Si (atom)	BET surface area ($m^2\ g^{-1}$)		S_{550}–S_{900}/S_{550} (%)
			550 °C/5 h[a]	900 °C/6 h	
Ce–Zr–O	0	1:1:0	101	40	60
Ce–Zr–Si(2.5)–O	2.5	1:1:0.28	145	60	59
Ce–Zr–Si(5.2)–O	5.2	1:1:0.62	149	88	41
Ce–Zr–Si(10)–O	10	1:1:1.34	179	110	39
Ce–Zr–Si(15)–O	15	1:1:2.32	306	142	54
Ce–Zr–Si(20)–O	20	1:1:3.68	313	153	51

[a] Calcination condition.

high temperature, the sintering degree (SD) is defined as $(S_{550}–S_{900})/S_{550}$, a decrease in the surface area fraction (or the surface area loss fraction) of the samples by the heat treatment at 900 °C for 6 h.

The results show that adding Si into the Ce–Zr–O solid solution can increase its surface area and decrease the sintering degree after calcination at high temperature. It is obvious that the surface area of the samples is a function of Si content. The higher the Si content, the larger the surface area is. When the Si content is more than 15 wt.%, the influence of increasing Si content on the surface area becomes weak, e.g. the surface area of Ce–Zr–Si(20)–O is only a little larger than that of Ce–Zr–Si(15)–O. For Ce–Zr–Si(10)–O and Ce–Zr–Si(5.2)–O calcined at 900 °C for 6 h, their SD (the surface area loss fraction) is the least (∼40%) among all samples. This means that the thermal-stability of Ce–Zr–Si–O solid solution with 5.2–10 wt.% Si is much higher.

As a comparison sample, pure silica was prepared with the same method as preparing the Ce–Zr–Si–O sample. After being calcined at 900 °C for 6 h, the surface area of pure silica is only 75 $m^2\ g^{-1}$ and much lower than that of Ce–Zr–Si–O samples. The results above show that, the presence of silica increases the surface area of the Ce–Zr–O sample by the coordinated interaction (or chemical combination) between SiO_2 and Ce–Zr–O solid solution, but the surface area of Ce–Zr–Si–O does not equal simply the summation of the surface area of SiO_2 and the surface area of Ce–Zr–O solid solution. This coordinated interaction leads to the formation of diffusion barrier layer that inhibits the coagulation of particles and change of pore structure. In fact, silicon is an effective element not only for improving the surface area and thermal-stability of Ce–Zr–O solid solution, but also for that of other metal oxides such as alumina [16–18].

3.2. XRD and laser Raman

Figs. 1 and 2 show the XRD patterns of the Ce–Zr–Si–O solid solutions calcined at 550 °C for 5 h and 900 °C for 6 h, respectively. The results show that, all the samples display a single crystalline phase of CeO_2–ZrO_2 solid solution. Because of different Si content, the crystalline form of the sample calcined at 550 °C for 5 h (Fig. 1) is different. By comparing with the XRD spectra of tetragonal $Ce_{0.5}Zr_{0.5}O_2$ phase (JCPDS file 8-1436, $2\theta = 29.24°$, 48.89°, 48.73°, 34.03°, 58.02°, 33.77°, and 57.67°) and the cubic phase (JCPDS file 8-221, $2\theta = 28.97°$, 48.13°, 57.13°, 33.60°, 59.94°, 77.85°, and

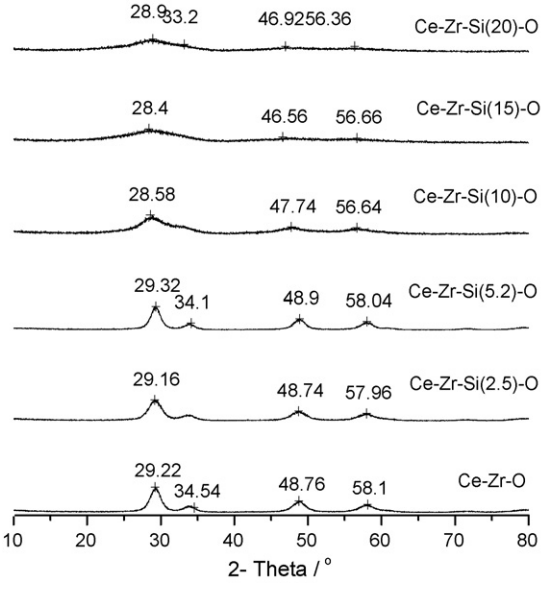

Fig. 1. XRD patterns of the samples calcined at 550 °C for 5 h.

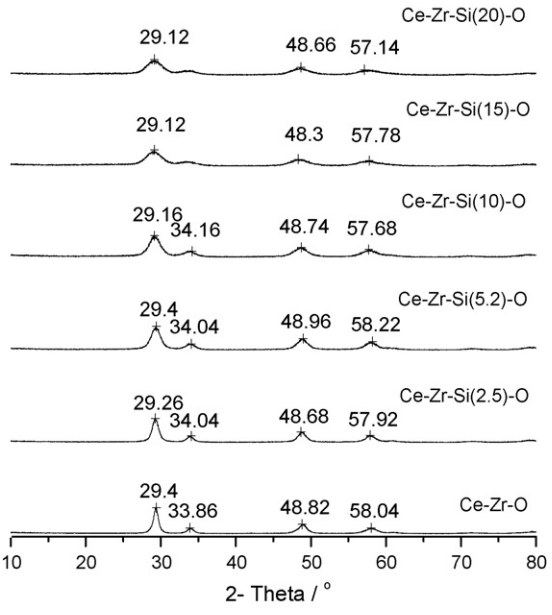

Fig. 2. XRD patterns of the samples calcined at 900 °C for 6 h.

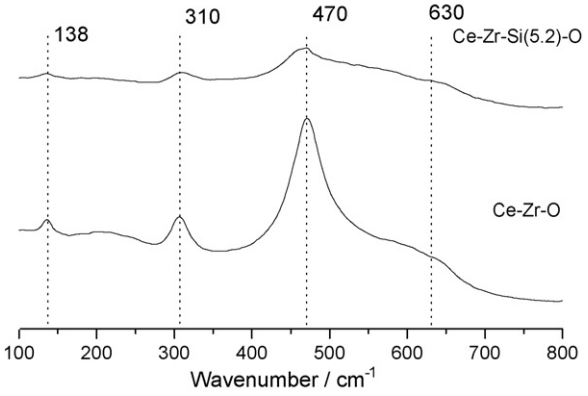

Fig. 3. Raman spectra of Ce–Zr–O and Ce–Zr–Si(5.2)–O after being calcined at 900 °C for 6 h.

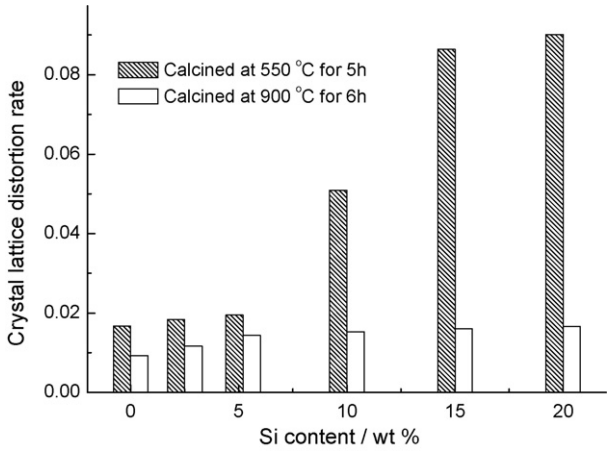

Fig. 4. Crystal lattice distortion rate as a function of the Si content and calcination temperature.

80.19°), when the Si content is 0–5.2 wt.% the sample displays the XRD spectrum of tetragonal $Ce_{0.5}Zr_{0.5}O_2$ phase; when the Si content is $\geq$10 wt.%, the crystalline form of the sample translates gradually the cubic phase, and the XRD diffraction peaks of the sample become weak and wide with the increase of Si content.

Fig. 2 shows the XRD spectra of the samples calcined at 900 °C for 6 h. These diffraction peaks are corresponding to that of tetragonal $Ce_{0.5}Zr_{0.5}O_2$, which is further affirmed by laser Raman analysis (Fig. 3). Like the samples calcined at 550 °C (Fig. 1), the XRD diffraction peaks of the samples calcined at 900 °C for 6 h become weak and wide with the increase of Si content.

In contrast to the XRD patterns that give information related mainly to the cation sublattice, Raman spectrum is dominated by an oxygen lattice vibration [19], and is sensitive to the crystalline symmetry, thus it is a useful tool to obtain the additional structural information of the multioxide system exhibiting lattice disorder. Fig. 3 shows the Raman spectra of Ce–Zr–O and Ce–Zr–Si(5.2)–O after being calcined at 900 °C for 6 h. Four absorption bands at approximately 630, 470, 310, 140 cm^{-1} are observed for two samples, and the presence of Si in Ce–Zr–O weakens its absorption peaks. It is known that pure ceria and Ce–Zr–O solid solution with a high content of cerium have a strong broad single peak at about 460 cm^{-1} due to the F_{2g} Raman-active mode of cubic fluorite structure [20,21]. Therefore, the Ce–Zr–O and Ce–Zr–Si(5.2)–O samples after being calcined at 900 °C for 6 h exist mainly as the tetragonal phase rather than the cubic phase.

As the oxygen exchange capacity of the sample is associated with its crystallinity and defects, a high crystallinity and few defects would decrease an oxygen exchange capacity of sample [11]. The higher the crystal lattice distortion rate of sample, the lower its cystallinity and more its defects are. Therefore, increasing the crystal lattice distortion rate of sample is very important to enhance its oxygen exchange capacity. The distortion rate (e) of crystal lattice is estimated by $e = 1/4\beta \operatorname{ctg} \theta$, β is the corrected peak width. The results in Fig. 4 show that, the crystal lattice distortion rate of Ce–Zr–O solid solution is promoted by addition of Si, which is induced by the cation size mismatch, e.g. the radius of Ce^{4+} = 0.097 nm, Zr^{4+} = 0.084 nm, Si^{4+} = 0.0226 nm. For the sample calcined at 550 °C, the crystal lattice distortion rate increases obviously with an increase of Si content. After being calcined at 900 °C, the crystal lattice distortion rate of the samples decreases obviously, but that of Ce–Zr–Si–O is still higher than that of Ce–Zr–O.

3.3. H_2-TPR

The TPR spectra of the samples are shown in Figs. 5 and 6, and their reducibility characteristic data derived from these spectra are listed in Table 2, including the peak top temperature (TT), reduction degree (RD), amount of hydrogen consumption (HC) and oxygen release (OR). The peak top temperatures of the samples calcined at 550 °C for 5 h are almost same

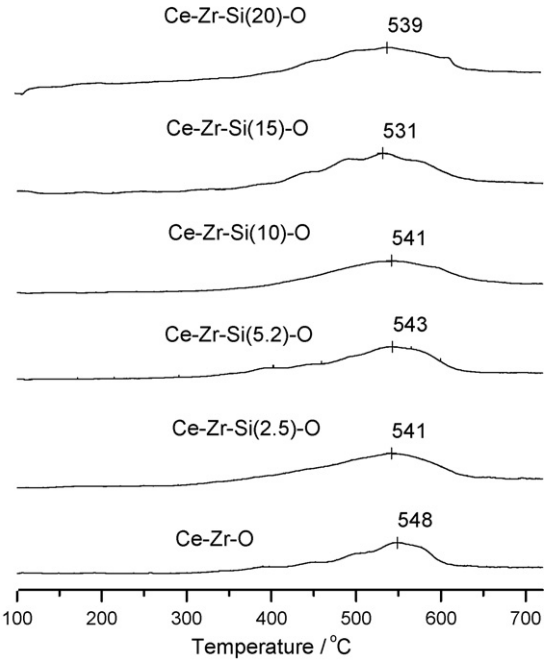

Fig. 5. TPR spectra of the samples calcined at 550 °C for 5 h.

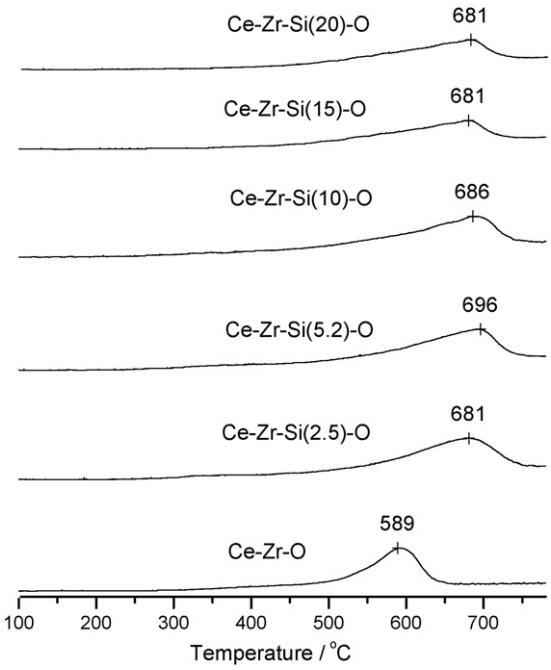

Fig. 6. TPR spectra of the samples calcined at 900 °C for 6 h.

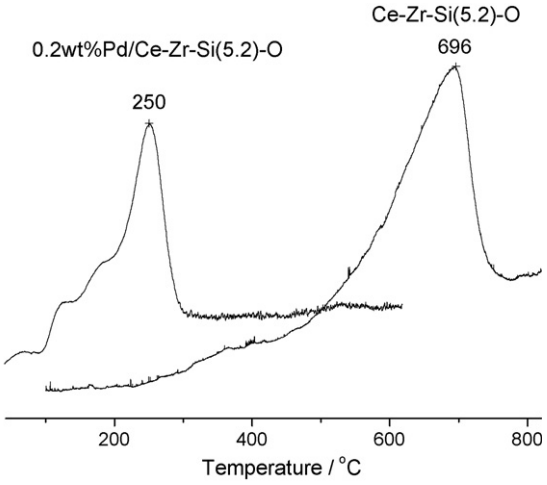

Fig. 7. TPR spectra of 0.2%Pd/Ce–Zr–Si(5.2)–O and Ce–Zr–Si(5.2)–O after being calcined at 900 °C for 6 h.

(∼540 °C), which can describe the reducibility of the bulk oxygen. The reduction of the surface oxygen generally occurs at <400 °C, but it cannot be distinguished from the reduction of the bulk oxygen clearly. However, the reduction degree, hydrogen consumption and oxygen release amount of different sample are much different, because of the different Si content introduced into the solid solutions. When the Si content is 5.2–10 wt.%, RD, HC and OR of the sample calcined at 550 °C for 5 h reaches 93–94%, 468 mmol/mol Ce and 234 mmol/mol Ce, respectively. After the samples are calcined at 900 °C for 6 h, their RD, HC and OR decreases obviously, however those of Ce–Zr–Si(5.2)–O and Ce–Zr–Si(10)–O are still highest among all samples.

The results above show that the presence of Si can increase the reducibility of Ce–Zr–O solid solution, but the content of Si added should be controlled to 5–10 wt.%. Further increase of Si content is unfavorable for the reducibility of Ce–Zr–O solid solutions.

Because of the higher reduction temperature of the solid solution, generally speaking, it cannot be used singly as a catalyst and it is often used together with other active components, such as, Pd, Pt and so on. Fig. 7 shows that the TPR spectra of 0.2% Pd/Ce–Zr–Si(5.2)–O and Ce–Zr–Si(5.2)–O. The results show that the presence of 0.2% Pd makes the top temperature of reduction peak decrease from 696 to 250 °C.

3.4. FT-IR

As shown in Fig. 8, there are an intense asymmetric absorption peak at 1110 cm^{-1} with a shoulder at ∼1220 cm^{-1} and two absorption peaks at 804 and 464 cm^{-1} in the FT-IR spectrum of pure SiO_2 prepared by reverse microemulsion method and calcined at 900 °C for 6 h. These features are related to strongly bonded Si–O–Si bridges in typical SiO_2 [22]. Moreover, a progressive variation in the Si–O–Si bonds can also be observed in the Si-doped Ce–Zr–O solid solutions as a function of the silicon content, with the help of the IR spectra. In the IR spectra of the Ce–Zr–Si(10–20)–O samples, the similar four peaks as that of SiO_2 still exist, but their relative intensities have changed and the peak at 1110 cm^{-1} has shifted a little to lower bands. For the Ce–Zr–Si(2.5)–O and Ce–Zr–Si(5.2)–O samples, the absorption peaks at 804 and 464 cm^{-1} have disappeared and the peak at 1110 cm^{-1} shift to much lower band. This means that, the Si–O–Si bridges of SiO_2 in the Ce–Zr–Si–O solid solution has changed comparing with SiO_2.

Table 2
Reductibility characteristic data of the samples

Sample	550 °C/5 h[a]				900 °C/6 h			
	TT/°C	RD/%	HC/mmol $(molCe)^{-1}$	OR/mmol $(molCe)^{-1}$	TT (°C)	RD (%)	HC/mmol $(molCe)^{-1}$	OR/mmol $(mol\ Ce)^{-1}$
Ce–Zr–O	548	75	376	188	589	68	340	170
Ce–Zr–Si(2.5)–O	541	85	424	212	681	70	352	176
Ce–Zr–Si(5.2)–O	543	93	468	234	696	75	376	188
Ce–Zr–Si(10)–O	541	94	468	234	686	75	372	186
Ce–Zr–Si(15)–O	531	73	364	182	680	66	332	166
Ce–Zr–Si(20)–O	539	73	364	182	681	69	344	172

[a] Calcination condition. TT: peak top temperature, RD: reduction degree, HC: hydrogen consumption, OR: oxygen release.

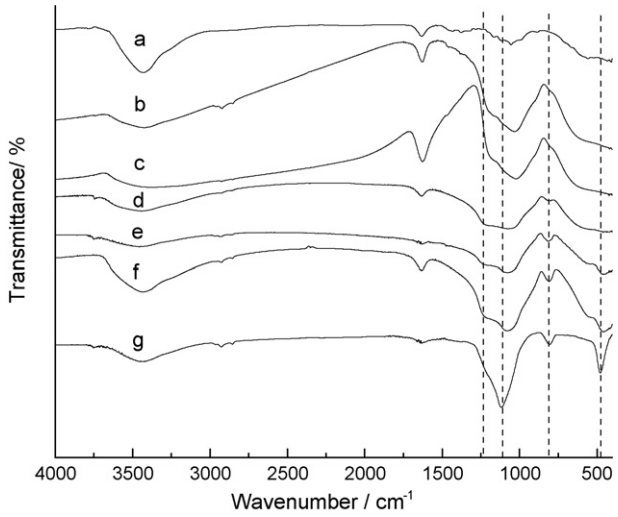

Fig. 8. FT-IR spectra of Ce–Zr–Si–O and SiO_2 (g) calcined at 900 °C for 6 h. The Si content is 0% (a), 2.5% (b), 5.2% (c), 10% (d), 15% (e) and 20% (f).

This is caused by the formation of Si–O–M (Ce or Zr) bridges in the Ce–Zr–Si–O solid solution.

According to the FT-IR spectra characters mentioned above, the Ce–Zr–Si–O solid solutions can be classified into three groups. Ce–Zr–Si(15)–O and Ce–Zr–Si(20)–O belong to one group, in which the IR absorption characters of Si–O–Si bonds changed a little comparing with pure SiO_2. Ce–Zr–Si(2.5)–O and Ce–Zr–Si(5.2)–O belong to another group, in which IR absorption characters of Si–O–Si bonds changed much. For the Ce–Zr–Si(10)–O sample, the change of IR absorption characters of Si–O–Si bonds is between the two groups above. These results show that, when Si content in the samples is lower, almost all Si atoms can be incorporated into the solid solution, leading to a great change of Si–O–Si bonds vibration; when Si content is higher, only a part of Si atoms can be incorporated into the solid solution, and the Si–O–Si bonds vibration still holds partly.

On the other hand, the calcination temperature can also influence the presence state of silicon in the samples. When the sample was calcined at 550 °C, the absorption peak at 1110 cm^{-1} shifts to near 1000 cm^{-1} and no peaks at 804 and 464 cm^{-1} can be observed (Fig. 9), because a high temperature leads to thermal shrinkage of the pore structure and a change of the intensity of Si–O–Si and Si–O–M bonds [23]. And the interaction (or chemical combination) between Si atoms and Ce–Zr–O solid solution can also be strengthened by the calcination at high temperature.

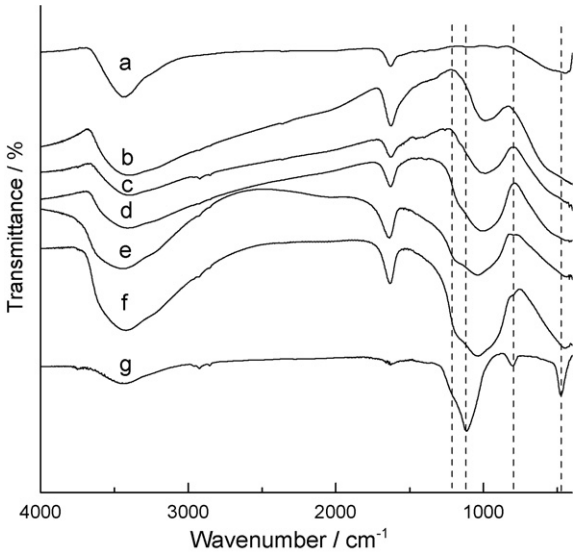

Fig. 9. FT-IR spectra of Ce–Zr–Si–O calcined at 550 °C for 5 h. The Si content is 0% (a), 2.5% (b), 5.2% (c), 10% (d), 15% (e) and 20% (f), and pure SiO_2 calcined at 900 °C for 6 h (g).

3.5. ^{29}Si MAS NMR

Ce–Zr–Si(20)–O was chosen as the model sample to be characterized by the solid NMR technique, because higher Si content in the sample can make ^{29}Si NMR signals more clearly. Fig. 10 shows the ^{29}Si NMR spectra of pure SiO_2 and Ce–Zr–Si(20)–O after being calcined at 900 °C for 6 h. In the spectrum of pure SiO_2, there are the main peak of Q^4 at −110 ppm (chemical shifts) and the shoulder peak of Q^3 at −98 ppm. For the pure SiO_2, the Q^n notification represents the silicon with $Si(OSi)_n(OH)_{4-n}$. The higher intensity of Q^4 indicates the condensation of Si–O–Si bonds [24,25], which is confirmed by the FT-IR absorption spectra. In the ^{29}Si NMR spectrum of Ce–Zr–Si(20)–O, the peak at −106 ppm is predominant and is assigned to T^3 of $Si(OSi)_3(OM)$. This T^3 peak is also often observed in the M-MCM molecular sieves such as Fe-MCM and Zr-HMS [26,27]. It is confirmed that the bridging of Si–O–M (M=Ce or Zr) bonds are formed. Other two peaks at −80 and −89 ppm can be attributed to T^1 and T^2, respectively.

3.6. XPS

In order to verify the surface composition and oxidation state of elements, the Ce–Zr–Si–O solid solutions were further

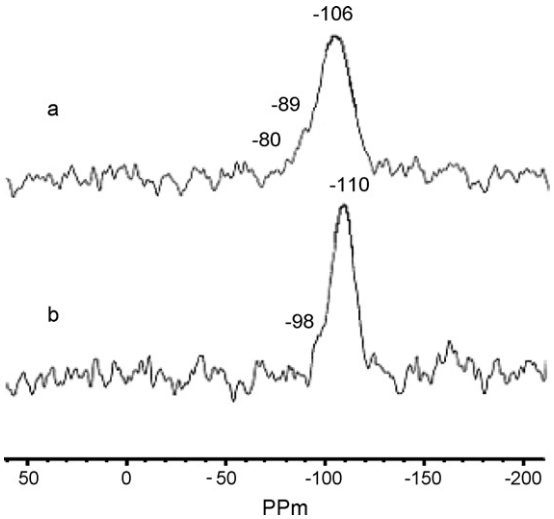

Fig. 10. ^{29}Si NMR spectra of Ce–Zr–Si(20)–O (a) and pure SiO_2 (b) after being calcined at 900 °C for 6 h.

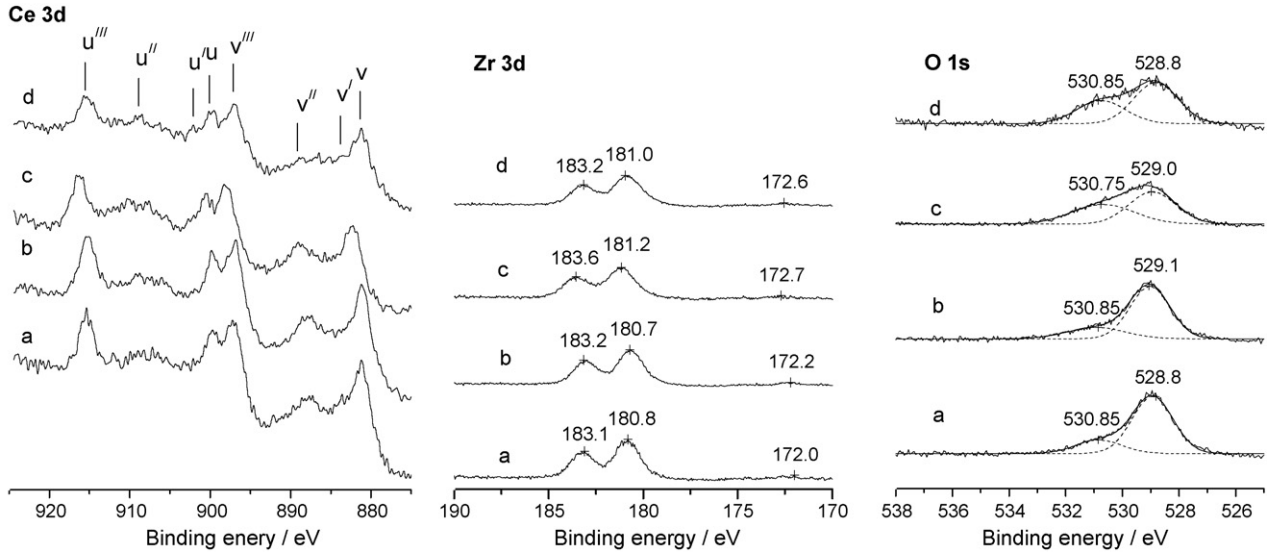

Fig. 11. XPS spectra of Ce–Zr–O calcined at 550 °C/5 h (a) or at 900 °C/6 h (b), and Ce–Zr–Si(5.2)–O calcined at 550 °C/5 h (c) or at 900 °C/6 h (d).

analyzed by XPS. On account of the higher thermal-stability and reducibility of Ce–Zr–Si(5.2)–O, it was used as a model sample and its XPS spectra were shown in Fig. 11. The Ce 3d spectrum can be resolved into eight components [28–30] and their binding energies (BE) are summarized in Table 3. The bands labeled v represent collectively Ce $3d_{5/2}$ and the bands labeled u represent Ce $3d_{3/2}$. The band labeled with v', v'', v''', u', u'' and u''' are attributed to Ce^{4+} and the band labeled with v' and u' are due to the presence of Ce^{3+}.

As shown in Fig. 11 (Ce 3d), the bands labeled with v' and u' cannot be distinguished clearly, which indicates that cerium in all the samples exists mainly in Ce^{4+}. And the BE of cerium is affected unobviously by addition of silicon and the calcination condition. The BE difference (18.4–19.0 eV) between Ce $3d_{3/2}$ and Ce $3d_{5/2}$ is also in agreement with an expected value of 18.6 eV [28].

The XPS spectra of Zr $3d_{3/2}$ and Zr $3d_{5/2}$ are shown in Fig. 11 (Zr 3d). The bands at 180.7–181.2 eV is ascribed to Zr $3d_{5/2}$, and the bands at 183.1–183.6 eV represent Zr $3d_{3/2}$. All these bands belong to Zr^{4+}, and the BE of zirconium is hardly affected by addition of silicon and the calcination condition.

As shown in Fig. 11 (O 1s), the O 1s XPS spectra are fitted with two peaks contributions. One peak at BE = 530.7–530.8 eV can be ascribed to adsorbed oxygen or hydroxyl-like groups (BE = 531.0 eV), and not to the O 1s of SiO_2 (BE = 532–533 eV). The other peak at BE = 528.8–529.0 eV may belong to lattice oxygen O^{2-} in Ce–Zr–O solid solutions [3,31–34]. But it is impossible to distinguish the difference between the oxygen anions associated with cerium and zirconium complexes.

In order to understand the effect of adding Si in the Ce–Zr–O solid solution on the amount of adsorbed oxygen or hydroxyl-like groups on the surface, their relative content in the total oxygen peaks was estimated by the peak area and shown in Table 4. The results show that the amount (area %) of adsorbed oxygen or hydroxyl-like groups on the Si-doped Ce–Zr–O solid solutions is much higher than that on single Ce–Zr–O solid solution, which implies the presence of silicon can increase noticeably the amount of adsorbed oxygen (or hydroxyl-like groups) on the surface of Ce–Zr–O solid solution.

Table 4
Area percent of adsorbed oxygen or hydroxyl-like groups in the O 1s peak of XPS spectra

Sample	Area percent of adsorbed oxygen or hydroxyl-like groups (%)
Ce–Zr–O	
550 °C/5 h[a]	21
900 °C/6 h	24
Ce–Zr–Si(5.2)–O	
550 °C/5 h	45
900 °C/6 h	38

[a] Calcination condition.

Table 3
Summary of the binding energies of Ce 3d in the XPS spectra

Sample	Calcination condition	Binding energy (eV)							
		u'''	u''	u'	u	v'''	v''	v'	v
Ce–Zr–O	550 °C/5 h	916.0	909.4	–	900.8	897.9	887.9	–	881.8
Ce–Zr–O	900 °C/6 h	916.0	909.5	–	900.5	897.4	888.0	–	881.8
Ce–Zr–Si(5.2)–O	550 °C/5 h	916.2	910.0	–	900.6	898.2	888.2	–	882.2
Ce–Zr–Si(5.2)–O	900 °C/5 h	916.3	909.6	–	900.2	897.6	887.8	–	881.8

4. Conclusions

To summarize the effect of silicon on the structure characteristics, thermal-stability and reducibility of Ce–Zr–O solid solutions, it is concluded that Si is a very effective additive for increasing the surface area and thermal-stability of Ce–Zr–O solid solution, but the presence of Si varies hardly the crystalline phase of the solid solution. For the 20 wt.% Si–Ce–Zr–O sample, its surface area reaches 153 $m^2 g^{-1}$ even after being calcined at 900 °C for 6 h. When 5.2–10 wt.% Si is added, the Ce–Zr–Si–O (Ce:Zr:Si = 1:1:0.6–1.3, atom) solid solution represents much higher thermal-stability, the reducibility of the Ce–Zr–O solid solution is promoted obviously, the reduction degree of the solid solution increase from 75% to 94% (from 68% to 75%) for the sample calcined at 550 °C for 5 h (at 900 °C for 6 h).

The modification of the structure, thermal-stability and reducibility of Si-doped Ce–Zr–O solid solution is due to the formation of Si–O–M (Ce or Zr) bonds and an increase of adsorbed oxygen or hydroxyl-like groups by adding silica into the Ce–Zr–O solid solution.

The crystal lattice defects and the crystal lattice distortion rate of the Ce–Zr–O solid solution are very two important factors for the excellent Ce–Zr–O solid solution, and can be increased obviously and stabilized easily by adding silica into the Ce–Zr–O solid solution.

Acknowledgements

This study was supported financially by the National Basic Research Program of China (2004CB719500), National Natural Science Foundation of China (20601008), Shanghai Rising-Star Program (05QMX1415) by The Commission of Science and Technology of Shanghai Municipality, and Rare Earths Office of Shanghai Municipality (200503).

Reference

[1] M. Shelef, R.W. McCabe, Catal. Today 62 (2000) 35.
[2] J. Kaspar, P. Fornasiero, N. Hickey, Catal. Today 77 (2003) 419.
[3] X. Wu, L. Xu, D. Weng, Appl. Surf. Sci. 221 (2004) 375.
[4] J. Kaspar, P. Fornasiero, J. Solid State Chem. 171 (2003) 19.
[5] T. Murota, T. Hasegawa, S. Aozaga, H. Matsui, M. Motoyama, J. Alloys Compd. 193 (1993) 73.
[6] Z. Hu, R.M. Heck, SAE paper 950254 (1995).
[7] J. Kasapa, P. Fornasiero, M. Graziani, Catal. Today 50 (1999) 285.
[8] M. Yashima, H. Arashi, M. Kakihana, M. Yoshimura, J. Am. Ceram. Soc. 77 (1994) 1067.
[9] G. Vlaic, R. Di Monte, P. Fornasiero, E. Fonda, J. Kaspar, M. Graziani, J. Catal. 182 (1999) 378.
[10] M. Che, C.O. Bennet, Adv. Catal. 36 (1989) 55.
[11] H. Schulz, W.J. Stark, M. Maciejewski, S.E. Pratsinis, A. Baiker, J. Mater. Chem. 13 (2003) 2979.
[12] M. Fernández-García, A. Martínez-Arias, A. Guerrero-Ruiz, J.C. Conesa, J. Soria, J. Catal. 211 (2002) 326.
[13] M. Chen, P. Zhang, X. Zheng, Catal. Today 93–95 (2004) 671.
[14] L.N. Ikryannikova, G.L. Markaryan, A.N. Kaharlanov, E.V. Lunia, Appl. Surf. Sci. 207 (2003) 100.
[15] X. Wang, Y. Guo, G. Lu, Y. Guo, Y. Wang, Z. Zhang, X. Liu, J. Rare Earths 22 (2004) 763.
[16] X. Wang, G. Lu, Y. Guo, Y. Wang, Y. Guo, Mater. Chem. Phys. 90 (2005) 225.
[17] T. Horiuchi, L. Chen, T. Osaki, T. Sugiyama, K. Suzuki, T. Mori, Catal. Lett. 58 (1999) 89.
[18] T. Horiuchi, T. Osaki, T. Sujiyama, K. Suzuki, T. Mori, J. Non-Cryst. Solids 291 (2001) 187.
[19] J.R. Ferraro, K. Nakamoto, Introductory Raman Spectroscopy, Academic Press, New York, 1994.
[20] A. Cabañas, J.A. Darr, E. Lester, M. Poliakoff, J. Mater. Chem. 11 (2001) 561.
[21] D.J. Kim, H.J. Jung, I.N. Yang, J. Am. Ceram. Soc. 76 (1993) 2106.
[22] R. Campostrinil, M. Ischia1, L. Armelao, J. Therm. Anal. Calorim. 78 (2004) 657.
[23] C.A. Koh, R. Nooney, S. Tahir, Catal. Lett. 47 (1997) 199.
[24] K. Noble, A.B. Seddon, M.L. Turner, P. Chevalier, D.L. Ou, J. Sol-Gel Sci. Technol. 26 (2003) 419.
[25] R. Takahashi, S. Sato, T. Sodesawa, T. Azuma, J. Sol-Gel Sci. Technol. 31 (2004) 373.
[26] J.H. Choy, J.B. Yoon, H. Jung, J.H. Park, J. Porous Mater. 11 (2004) 123.
[27] Z. Yuan, S. Liu, T. Chen, J. Wang, H. Li, J. Chem. Soc. Commun. 9 (1995) 973.
[28] P. Burroughs, A. Hamnett, A.F. Orchard, J. Chem. Soc., Dalton Trans. (1976) 1686.
[29] D.I. Kondarides, X.E. Verykios, J. Catal. 174 (1998) 55.
[30] F.B. Noronha, E.C. Fendley, R.R. Soares, W.E. Alvarez, D.E. Resasco, J. Chem. Eng. 82 (2001) 25.
[31] P. Ciambelli, S. Cimino, S. De Rossi, M. Faticanti, L. Lisi, G. Minelli, I. Pettiti, P. Porto, G. Rosso, M. Turco, Appl. Catal. B 24 (2000) 243.
[32] M.W. Roberts, Chem. Soc. Rev. 18 (1989) 451.
[33] N. Gunasekaran, S. Rajadurai, J.J. Carberry, N. Bakshi, C.B. Alcock, Solid State Ionics 73 (1994) 289.
[34] K. Tabata, I. Matsumato, S. Kohihi, J. Mater. Sci. 22 (1998) 1882.